

## **Title**

Agent-Based Uncertainty Awareness Improves Automated Radiology Report Labeling with an Open-Source Large Language Model

## **Authors**

1. Hadas Ben-Atya (MS), Faculty of Biomedical Engineering, Technion - Israel Institute of Technology, Haifa, Israel.
2. Naama Gavriellov, Faculty of Biomedical Engineering, Technion - Israel Institute of Technology, Haifa, Israel.
3. Zvi Badash, Faculty of Data and Decision Sciences, Technion - Israel Institute of Technology, Haifa, Israel.
4. Gili Focht (MSc), Juliet Keidan Institute of Pediatric Gastroenterology Hepatology and Nutrition, Shaare Zedek Medical Center, The Hebrew University School of Medicine, Jerusalem, Israel.
5. Ruth Cytter-Kuint (MD), Pediatric Radiology Unit, Radiology Department, The Eisenberg R&D Authority, Shaare Zedek Medical Center, The Hebrew University of Jerusalem, Jerusalem, Israel.
6. Talar Hagopian (MD), Pediatric Radiology Unit, Radiology Department, The Eisenberg R&D Authority, Shaare Zedek Medical Center, The Hebrew University of Jerusalem, Jerusalem, Israel.
7. Dan Turner (MD PhD), Juliet Keidan Institute of Pediatric Gastroenterology Hepatology and Nutrition, Shaare Zedek Medical Center, The Hebrew University School of Medicine, Jerusalem, Israel.
8. Moti Freiman (PhD), Faculty of Biomedical Engineering, Technion - Israel Institute of Technology, Haifa, Israel.

## **Corresponding author contact information**

E-mail address: [moti.freiman@technion.ac.il](mailto:moti.freiman@technion.ac.il)

Full address: Technion, Faculty of Biomedical Engineering, Silver Building, 3200001

## **Funding information**

The study was sponsored by the Leona M. and Harry B. Helmsley Charitable Trust. The funders had no role in the study design, data collection and analysis, decision to publish, or preparation of the manuscript.

## **Abstract:**

**Purpose:** To improve the reliability and performance of Large Language Models (LLMs) in extracting structured data from radiology reports, particularly in domains with complex and non-English texts (e.g., Hebrew), by incorporating agent-based uncertainty-awareness method to achieve trustworthy predictions in medical applications.

## **Materials and Methods:**

This retrospective study analyzed 9,683 Hebrew radiology reports from Crohn's disease patients (2010–2023) across three medical centers. A subset of 512 reports was manually annotated for six gastrointestinal organs and 15 pathological findings, while the remaining data was automatically annotated using the HSMP-BERT model.

Structured data extraction used Llama 3.1 (Llama 3-8b-instruct), an open-source LLM, with Bayesian Prompt Ensembles (BayesPE) leveraging six semantically equivalent prompts for uncertainty estimation. An Agent-Based Decision Model synthesized multiple prompt outputs into five confidence levels for calibrated uncertainty, compared against three entropy-based models. Performance was assessed via accuracy, F1 score, precision, recall, and Cohen's Kappa, both before and after filtering high-uncertainty cases.

**Results:** The agent-based model outperformed the baseline across all metrics, achieving an F1 score of 0.3967, recall of 0.6437, and Cohen's Kappa of 0.3006. After filtering high uncertainty cases ( $\geq 0.5$ ), the F1 score increased to 0.4787 and Kappa to 0.4258. Uncertainty histograms

showed clear separation between correct and incorrect predictions, with the agent-based model exhibiting the best-calibrated uncertainty predictions.

**Conclusion:** Incorporating uncertainty-aware prompt ensembles and an agent-based decision model significantly enhances the performance and reliability of LLMs in structured data extraction from radiology reports, offering a calibrated and interpretable approach for high-stakes medical applications.

### **Summary Statement:**

An uncertainty-aware approach using prompt ensembles and an agent-based decision model improved the reliability, interpretability, and performance of LLMs in extracting structured data from radiology reports, with calibrated predictions and enhanced metrics.

### **Key Points:**

- Bayesian prompt ensembles improved accuracy and reliability in extracting structured data from Hebrew radiology reports, with the agent-based decision model achieving top performance (F1: 0.4787, Kappa: 0.4258).
- Uncertainty-aware filtering enhanced metrics and clearly distinguished correct from incorrect predictions, as shown by calibrated uncertainty histograms.
- The agent-based decision model delivered robust, interpretable results by synthesizing multiple prompts and categorizing decisions by confidence levels.

### **Keywords:**

Deep Learning; LLM; Uncertainty Estimation; Radiology Report;

## **Introduction:**

Radiology reports contain critical clinical information, essential for healthcare decision-making, retrospective studies, and radiologic image annotation. Despite ongoing efforts to implement structured reporting [1], unstructured free-text reports remain dominant, posing challenges for large-scale data analysis due to their variability and lack of standardization. Automating the extraction of structured data addresses these issues by streamlining workflows, reducing manual effort, and improving data consistency and accessibility. This approach not only enhances patient care but also enables large-scale research through comprehensive meta-analyses, accelerated scientific discoveries, and stronger evidence-based practice [2-4].

Large language models (LLMs) can automate structured data extraction from radiology reports by processing unstructured text to efficiently yield clinically relevant insights [5-7]. However, privacy concerns around sensitive medical data have prompted interest in open-source LLMs, which offer greater transparency, adaptability, and control. Models like Llama 3.1 can extract meaningful insights from medical texts while mitigating risks associated with proprietary systems [8].

Despite their potential, applying LLMs to radiology remains challenging. Overconfidence in predictions undermines reliability in high-stakes medical contexts [9], highlighting the need for robust methods to assess and manage uncertainty. Additional obstacles arise in underrepresented languages like Hebrew, where limited high-quality training data hampers performance. Innovative strategies to enhance LLM adaptability and reliability are essential for effective deployment across diverse linguistic and clinical settings.

Recent progress in uncertainty quantification enhances LLM reliability and interpretability in high-stakes domains like healthcare and radiology. Techniques such as Confidence Elicitation (CE) [10-12], Token-Level Probabilities (TLP), and Sample Consistency (SC) address overconfidence by providing uncertainty measures. However, these approaches treat all responses with equal

weight may overlook variations in quality, relevance, or coherence. Refining these methods is crucial for meeting the demands of increasingly complex applications.

Bayesian Prompt Ensembles (BayesPE) [13] enhance uncertainty estimation in LLMs by combining semantically equivalent prompts and optimizing their weights via variational inference, improving prediction reliability and calibration. However, its reliance on a parametric model for prompt weights may limit flexibility in complex or dynamic settings.

Agent-based approaches [14] offer adaptive decision-making for LLM outputs, potentially addressing BayesPE's limitations by incorporating more sophisticated uncertainty estimation processes. This study aims, therefore, to introduce and evaluate an agent-based method for uncertainty-aware, LLM-based structured data extraction from real-world Hebrew radiology reports of Crohn's disease patients, comparing its performance and robustness to the probabilistic aggregation methods of BayesPE.

## **Materials and Methods:**

### **Data Collection**

The retrospective multicenter study was approved by the institutional review board. Informed consent was waived due to the retrospective nature of the study.

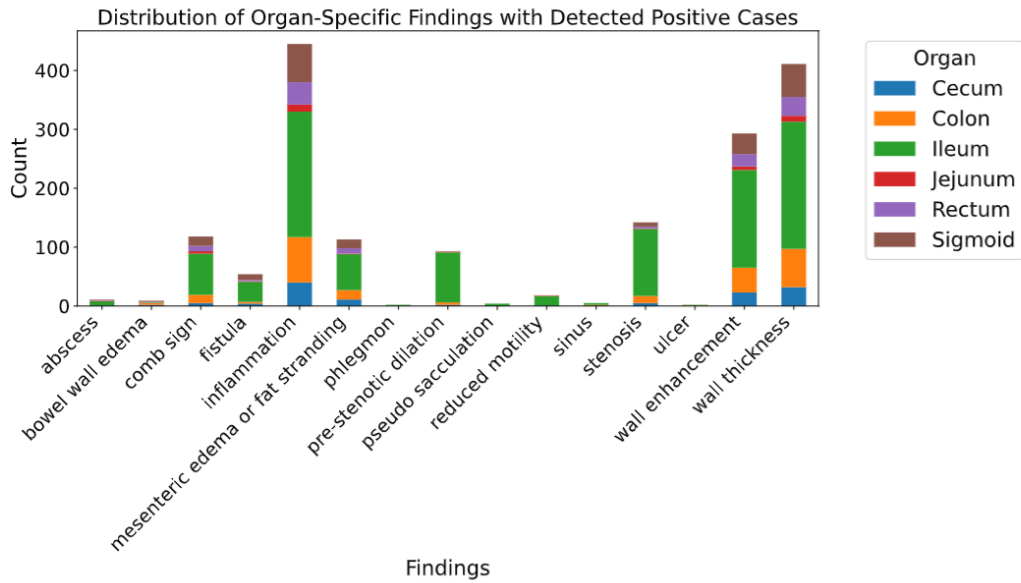
Free-text Hebrew radiology reports of Crohn's disease patients were sourced from the EPI-IIRN study [15]. The dataset comprises 9,683 reports, each corresponding to a patient visit, collected from 8,093 unique patients across three medical institutions. These reports document Magnetic Resonance Enterography or CT Enterography exams conducted between 2010 and 2023.

### **Manual Data Annotation**

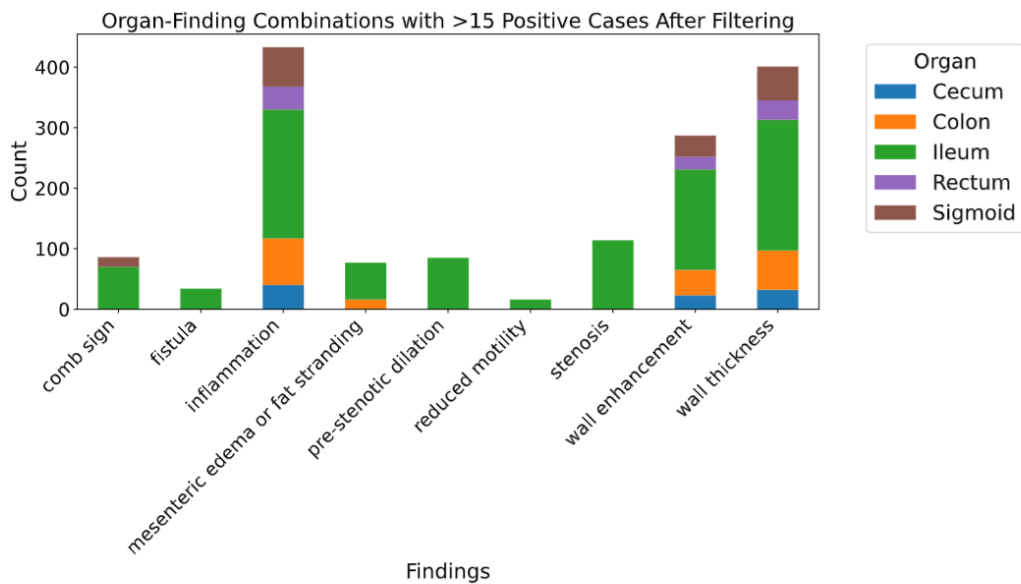
We randomly selected 512 reports from the dataset, each manually annotated by a trained radiologist (T.H.) for six gastrointestinal organs (Jejunum, Ileum, Cecum, Colon, Sigmoid, and Rectum). Each report included up to 15 distinct pathological findings (e.g., Inflammation, Wall thickening, Ulceration) [16], resulting in 90 organ–finding combinations. Labels were assigned as 0 (negative), 1 (positive), 2 (organ absent due to surgery), or 9 (organ not visible on MRI). In the main experiment, we treated labels 2 and 9 as negative, leaving two possible outcomes per organ–finding combination. We excluded combinations with  $\leq 15$  positive cases, yielding 23 final organ–finding combinations. Fig. 1 shows the distribution of all organ-specific findings and the subset with at least 15 positive samples. Detailed information about the prevalence of the different labels in the test set is provided in Table S2 in the supplementary materials.

### **NLP Based Annotations**

We used HSMP-BERT, an in-house BERT-based NLP model for structured data extraction from Hebrew radiology reports of Crohn’s disease patients [17,18], to annotate the entire dataset of 9,683 reports. The model was trained on the manually annotated subset, focusing on 23 prevalent organ–finding combinations. Performance metrics for these labels appear in Appendix A. To ensure high-quality data for the BayesPE-based methods, we retained only labels with a Cohen’s Kappa score above 0.7, resulting in eight final labels: Ileum comb sign, Ileum inflammation, Ileum pre-stenotic dilation, Ileum stenosis, Ileum wall enhancement, Ileum wall thickness, Rectum wall thickness, and Sigmoid comb sign.



(a) Distribution of organ-specific findings with detected positive cases.



(b) Organ-finding combinations with 15+ positive cases after filtering.

**Fig. 1:** (a) Distribution of organ-specific findings and (b) filtered organ-finding combinations with more than 15 positive cases.

## Large Language Model (LLM) utilization for structured data extraction

We used the Llama 3.1 model (Llama 3-8b-instruct) [19], part of Meta's multilingual LLM collection, to extract structured data from Hebrew radiology reports. Although it supports several languages (English, German, French, Italian, Portuguese, Hindi, Spanish, Thai), Hebrew is not among them. Llama 3.1 utilizes an auto-regressive transformer architecture [20], further refined via supervised fine-tuning (SFT) [21] and reinforcement learning from human feedback (RLHF) [22-24] to better align with human preferences. Given its limited Hebrew support, we carefully adapted the model for this context.

We prompted the model with various organ–finding combinations to extract structured data from Hebrew radiology reports, asking whether a specific finding was indicated. We also included a self-explanation step for each answer, aiding model validation and improving accuracy, as previously demonstrated. Specifically, we used the following prompt:

### LLM Prompt example:

```
"Does the following radiology report indicate that the patient has {label}? Here is the report:
{{}}. Please provide a concise response in JSON format, adhering to the schema: {{'Answer':
'Yes/No', 'Explanation': 'str'}}. Important: Only return a single valid JSON response. For
instance: {{'Answer': 'Yes', 'Explanation': 'The report states that the patient has a severe case
of the disease.'}}"
```

## Uncertainty Estimation with Bayesian Prompt Ensembles

We employed the Bayesian Prompt Ensembles (BayesPE) method [13] to estimate uncertainty in LLM-generated predictions by leveraging an ensemble of semantically equivalent prompts, without modifying the LLM's architecture or requiring retraining. In alignment with their findings, we selected six prompts to balance the benefits of prompt diversity with computational efficiency,

as adding more prompts provided only marginal gains. We used ChatGPT [25] to design these six prompts, each with identical semantic intent to determine the presence of specific findings in radiology reports. This ensures consistency in task execution despite variations in wording. The complete prompt structures appear in Appendix B.

We developed an agent-based method and three entropy-based approaches to quantify model uncertainty using outputs from multiple prompts. Fig. 2 illustrates the different approaches we utilized to assess uncertainty.

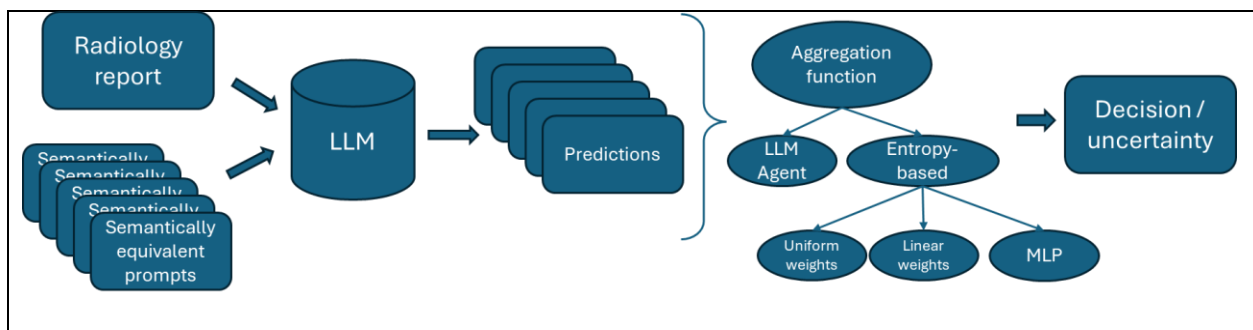


**Fig. 2:** Illustration of the proposed Bayesian Prompt Ensemble pipeline for uncertainty-aware predictions. A radiology report and multiple semantically equivalent prompts are fed into an LLM, generating one prediction per prompt. These predictions are then aggregated to yield a final decision and uncertainty estimation. The aggregation function can be either an LLM agent or an entropy-based function that applies uniform weights, learned fixed weights, or weights predicted by a pre-trained MLP model.

### 1. Agent Decision Model

We propose an Agent Decision Model to consolidate the outputs of multiple prompts, derive a final decision, and quantify its uncertainty. This model synthesizes responses and explanations from an ensemble of prompts, producing a unified decision with a rationale for its conclusion. The agent evaluates response consistency, assesses the clarity and coherence of explanations, and identifies indications of uncertainty. Based on these factors, it categorizes the final decision into one of five distinct confidence levels:

- Definitely Yes,
- Likely Yes,
- Definitely No,
- Likely No,
- Uncertain.

To ensure interpretability and structure, the agent outputs its decision and reasoning in a predefined JSON format: {"Decision": "str", "Explanation": "str"}. This formatting requirement ensures that the output is consistent and machine-readable. The agent receives as input a set of answers ("Yes" or "No") and their corresponding explanations generated by the LLM with the different prompts. The agent evaluates these inputs based on the consistency of the answers, the clarity of their explanations, and the degree of ambiguity to produce its final decision. In our implementation, we utilized the Llama 3 - 70B model as the agent. Its outputs include:

- A final decision (e.g., "Definitely Yes", "Likely No").
- An explanation for the decision, highlighting the key factors that influenced its reasoning.

The agent's uncertainty level is derived based on the confidence category of its decision:

- Definitely Yes/No: Uncertainty = 0
- Likely Yes/No: Uncertainty = 0.5
- Uncertain: Uncertainty = 1

This semi-quantitative approach enables the seamless integration of uncertainty measures into downstream analyses, enhancing the interpretability of the decision-making process. For the "Uncertain" response, a final "Yes" or "No" decision is determined by aggregating the probabilities for each option from the previous step and selecting the option with the highest overall score.

An example of two responses by the backbone LLM that are provided as input to the agent and an example of the agent output for the input responses presented are provided below.

#### Agent inputs (2 examples of the LLM output):

- **Answer:** "No".  
**Explanation:** "The report does not mention Cecum inflammation, but rather mentions air-filled bubbles in the soft tissue of the right abdomen, likely originating from the small intestine."
- **Answer:** "Yes".  
**Explanation:** "The report mentions the presence of bubbles or air pockets in the soft tissue of the right abdomen, which may be indicative of inflammation in the cecum."

#### Agent output:

- **"Decision":** "Likely No",  
**"Explanation":** "The majority of the answers (3 out of 4) suggest that there is no inflammation in the Cecum, and the explanations provided are clear and consistent. The one answer that suggests 'yes' is not strongly supported and appears to be an over-interpretation of the report."

## 2. Entropy-based Decision Models

Alongside our agent-based decision model, we implemented three entropy-based models for comparison. These models determine the final prediction and its entropy by applying different weighting methods to the prompt outputs, as follows:

- a) Uniform weights.
- b) Linearly optimized weights.
- c) Learnable weights using MLP.

We describe each in detail below.

**Uniform Weights:** In this approach, all prompts are assigned equal weights:

$$w_i = \frac{1}{\text{len(Prompts)}}$$

This method operates under the assumption of no prior knowledge regarding the efficacy of individual prompts, thus distributing trust uniformly across all prompts. Such an approach enhances simplicity and mitigates potential biases in weight assignment.

**Linearly Optimized Weights:** In this approach, we optimized the weights assigned to different prompts using a small validation set. We determine the weights by minimizing the following objective function:

$$L(w_{\text{raw}}, \log(P(y^*|a_i, x))) = \sum_{i=1}^N w_i \cdot \log(P(y^*|a_i, x)) - \sum_{i=1}^N w_i \log(w_i)$$

where  $y^*$  denotes the correct answer (e.g., "Yes" or "No"),  $a_i$  represents the  $i^{\text{th}}$  prompt structure, and  $x$  is the radiology report. The weights  $w_i$  are computed by applying a softmax transformation to the raw weights  $w_{\text{raw}}$ :

$$w_i = \frac{\exp(w_{\text{raw},i})}{\sum_{j=1}^N \exp(w_{\text{raw},j})}$$

The first term  $\sum_{i=1}^N w_i \cdot \log(p(y^*|a_i, x))$  represents the log-likelihood of the validation data, while the second term,  $\sum_{i=1}^N w_i \log(w_i)$ , acts as an entropy-based regularizer, discouraging overconfidence in a single prompt.

During inference, model uncertainty was estimated from the weighted entropy of the ensemble of prompts, representing the LLM's confidence in its predictions.

We performed linear optimization of prompt weights for each organ-finding label. We utilized a fixed subset of 50 samples from the manually annotated dataset. We conducted this process independently for each label, resulting in a distinct, fixed weight combination tailored to each organ-finding label.

**Learnable Weights Using MLP:** The uniform and linearly optimized weighting methods assume fixed or simple relationships between prompts, limiting their ability to capture complex interactions. To address this, we introduce a Multi-Layer Perceptron (MLP) for adaptive prompt weight optimization. The MLP dynamically adjusts weights based on prompt behavior across the dataset, enabling more accurate weighting in scenarios with intricate dependencies between prompts. The forward pass for the model is defined as follows:

$$w = \text{softmax}(\text{MLP}(h))$$

where  $h$  represents the fixed prompt embeddings, and  $w$  are the normalized weights.

The training objective combines the binary cross-entropy loss between the ground truth labels  $y_{gt}$  and the weighted prompt probabilities  $\hat{y}$ , with an entropy regularization term to encourage well-calibrated uncertainty:

$$\mathcal{L} = \text{BCE}(\hat{y}, y_{gt}) - \lambda \cdot \sum_i w_i \log(w_i)$$

where  $\lambda$  is a hyperparameter that controls the strength of the entropy regularization term.

The MLP is trained using the Adam optimizer, with gradient clipping applied to ensure stable updates. During inference, the final predicted probabilities for each label (yes/no) are the weighted average of the individual prompt probabilities:

$$\hat{y} = \sum_i w_i p_i$$

where  $w_i$  are the optimized weights, and  $p_i$  are the probabilities associated with each prompt. The final decision is the label with the highest probability. This adaptive approach offers a distinct advantage over simpler methods by dynamically adjusting the prompt weights, potentially improving performance and yielding better-calibrated uncertainty estimates.

We leveraged the automatically labelled cases for the 8 selected labels to train the MLP model. We used 60% of the automatically labelled dataset, comprising 5794 cases, for training, 20% for validation and 20% for internal test of the weights. We trained the MLP model across all labels simultaneously, producing a single model applicable to all labels. During inference, we used the trained MLP model to predict prompt weights dynamically for each case and each of the 23 organ-finding label combinations.

## **Evaluation Setup**

We evaluated our approach on the manually annotated test dataset (462 reports, with 23 organ-finding combinations), excluding the 50 cases used to tune the linear weights. To establish a baseline, we simulated using any single prompt from our set of six, computing performance metrics for each prompt independently and then averaging the results. We then compared various Bayesian aggregation methods with this baseline, both before and after filtering high-uncertainty cases. For each organ-finding label, we measured accuracy, F1, and Cohen's Kappa at two uncertainty thresholds: excluding samples above 0.5 and excluding up to 20% of samples if their uncertainty exceeded 0.5. We also generated uncertainty histograms for each model, separating correct and incorrect predictions, and reported the median uncertainty in each group to assess how well uncertainty levels distinguish between them.

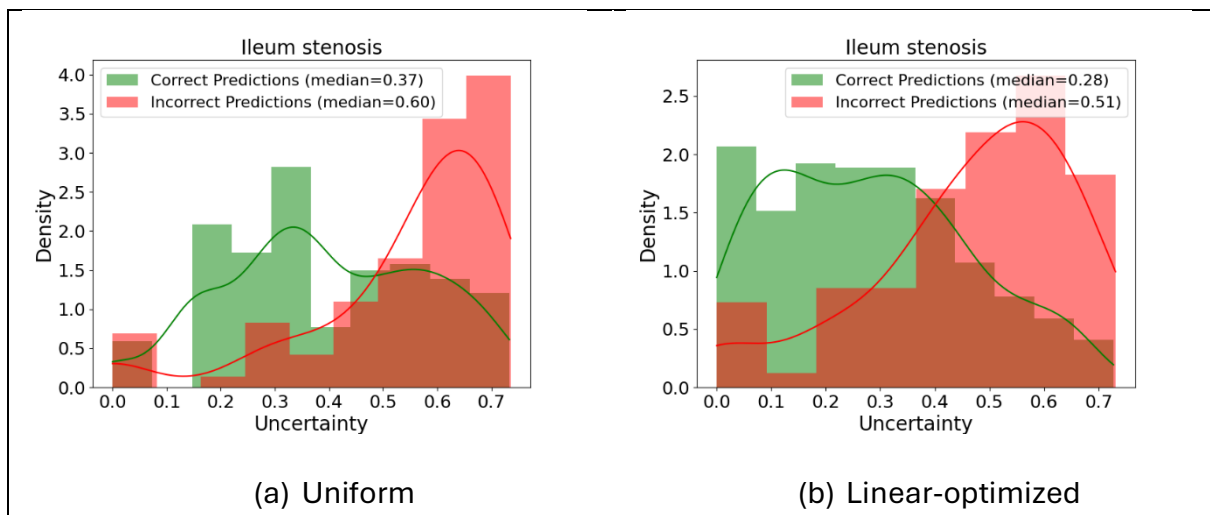
## **Results:**

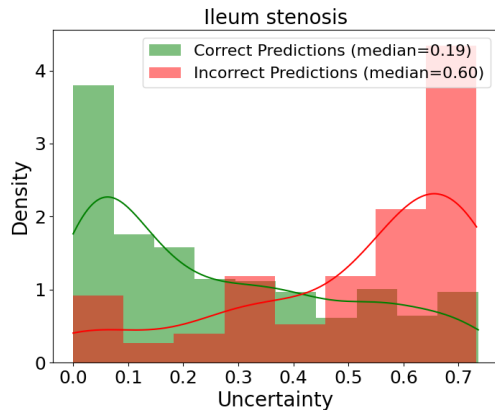
### **Uncertainty-aware prediction without filtering**

Table 1 shows that aggregating multiple prompts significantly outperforms using a single prompt. The baseline (single-prompt) model has the lowest metrics, particularly  $F1=0.2699$  and  $Kappa=0.1790$ . In contrast, the agent-based approach achieves the best overall balance, with  $F1=0.3967$ ,  $recall=0.6437$ , and  $Kappa=0.3006$ , suggesting it handles ambiguity effectively. Although the MLP model attains the highest accuracy (0.8605) and precision (0.3772), its recall is lower (0.3977). Both uniform and linear methods also surpass the baseline, with linear showing slightly higher accuracy (0.8454) for similar F1, emphasizing the benefits of weight-optimized prompt ensembles.

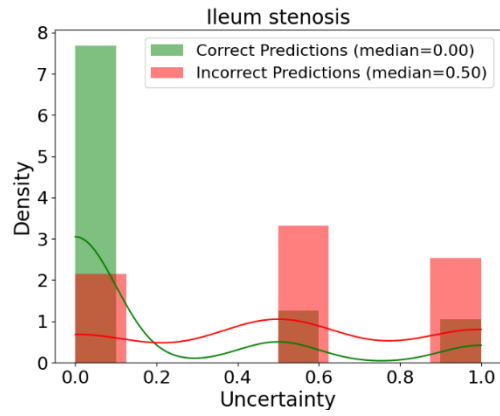
### Uncertainty Histograms

Figures 3 and 4 show the uncertainty histograms for two representative labels from the four methods, with the Agent model providing the clearest separation between correct and incorrect predictions. Additional histograms appear in Appendix D. Table 2 presents the average median uncertainty across all 23 labels, illustrating that a well-calibrated model should exhibit low uncertainty for correct predictions and high uncertainty for incorrect ones. The Agent model yields an average median uncertainty of 0.0 for correct predictions and about 0.5 for incorrect ones, indicating superior calibration compared to the other methods.





(c) Learnable - MLP



(d) Agent

**Fig. 3:** Uncertainty Histograms for Ileum stenosis Computed by: (a) Uniform Weights, (b) Linear-Optimized Weights, (c) Learnable- MLP Weights, and (d) Agent-based decision.

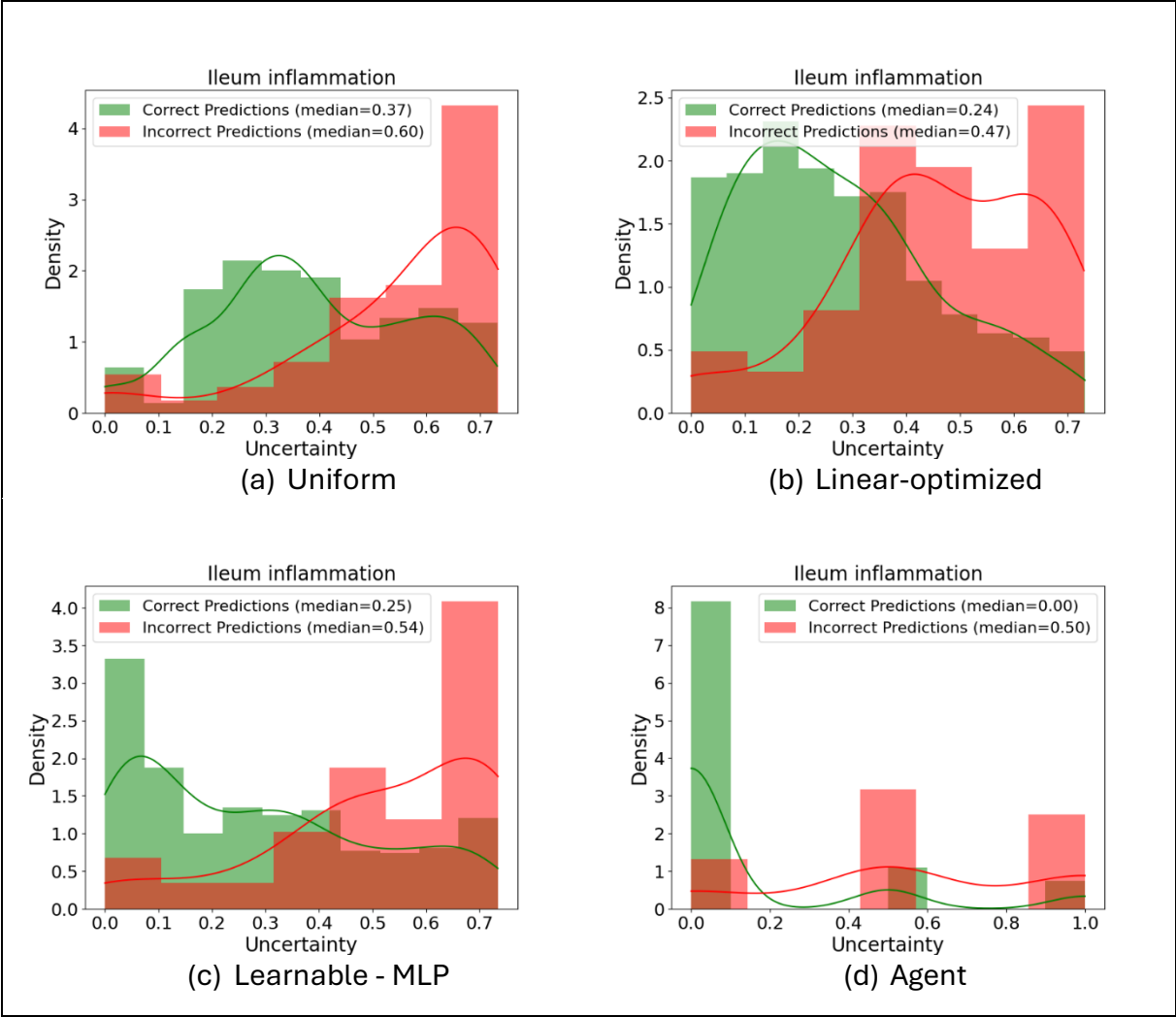


**Fig. 4:** Uncertainty Histograms for Ileum inflammation Computed by: (a) Uniform Weights, (b) Linear-Optimized Weights, (c) Learnable- MLP Weights, and (d) Agent-based decision.

## **Uncertainty-aware prediction with filtering**

Tables 3 and 4 present model performance after filtering out cases with uncertainty  $\geq 0.5$ . Table 3 imposes no cap on excluded cases, while Table 4 limits exclusion to at most 20%. In both scenarios, removing high-uncertainty cases improves accuracy, F1, and Cohen's Kappa. Appendix C provides additional tables summarizing the result per label and model.

With no exclusion cap (Table 3), the MLP model achieves the highest accuracy (92.42%), whereas the Agent approach yields the best F1 (47.87%) and recall (66.14%). Under the 20% cap (Table 4), MLP again leads in accuracy (90.87%), and the Agent method retains the highest F1 (44.94%) and recall (72.95%). These results highlight the Agent method's strong focus on identifying true positives while maintaining robust calibration, even with constrained exclusions.

### **Discussion:**

In this study, we evaluated prompt-ensemble-based uncertainty awareness for structured data extraction from radiology reports using LLMs. Aggregating predictions from multiple prompts and filtering high-uncertainty cases outperformed single-prompt methods, notably boosting F1 and Cohen's Kappa.

Among the tested approaches, the agent-based method provided the best overall balance in F1, recall, and Cohen's Kappa by integrating multiple prompts and accounting for their consistency. Meanwhile, the MLP model attained the highest precision and accuracy, useful for scenarios demanding fewer false positives, but its lower recall indicates some missed positive cases. This trade-off underscores the importance of selecting models based on task needs.

Additionally, the agent approach demonstrated superior calibration, distinguishing correct and incorrect predictions more effectively than other methods. Entropy-based metrics further confirmed the agent's robust handling of complex prompt outputs, enhancing prediction reliability.

Excluding high-uncertainty cases improved accuracy, F1, and Cohen's Kappa, showing the value of uncertainty-aware filtering for better alignment between model confidence and prediction correctness. Setting class-specific thresholds at the output layer can improve recall for minority classes while preserving precision for majority classes, thus optimizing performance for the target application.

Large language models (LLMs) efficiently automate structured data extraction from radiology reports by converting unstructured text into clinically relevant insights [5-7]. However, ensuring trustworthy application through robust uncertainty quantification remains an open challenge. While Zeng et al. [26] demonstrated the potential of multiple interacting LLM agents with specialized tasks to improve performance in medical applications, their role in quantifying uncertainty for reliable use remains underexplored. This study is the first to introduce a generalizable agent-based approach that quantifies uncertainty and fosters the trustworthy use of LLMs for structured data extraction from radiology reports.

Our study has limitations. First, while the focus was on radiology reports, extending these methods to LLM-based analysis of other medical reports, such as pathology reports or electronic medical records, requires additional validation. Second, optimizing ensemble techniques for highly imbalanced datasets remains a challenge. Future work should explore tailored approaches to address these limitations and investigate the application of uncertainty quantification in broader clinical scenarios.

In conclusion, our findings demonstrate the effectiveness of prompt ensembles-based uncertainty awareness in enhancing LLM performance for structured data extraction in radiology. The agent-based approach emerged as particularly robust, achieving superior results. Incorporating uncertainty quantification not only improves reliability but also facilitates interpretability, paving the way for more impactful and trustable AI applications in healthcare.

## **References:**

1. Nobel JM, van Geel K, Robben SG. Structured reporting in radiology: a systematic review to explore its potential. *European Radiology*. 2022;1-18.
2. Hassanpour S, Langlotz CP. Information extraction from multi-institutional radiology reports. *Artificial Intelligence in Medicine*. 2016;66:29-39.
3. Haendel MA, Chute CG, Robinson PN. Classification, ontology, and precision medicine. *New England Journal of Medicine*. 2018;379(15):1452-62.
4. Langlotz CP, Allen B, Erickson BJ, Kalpathy-Cramer J, Bigelow K, Cook TS, et al. A roadmap for foundational research on artificial intelligence in medical imaging: from the 2018 NIH/RSNA/ACR/The Academy Workshop. *Radiology*. 2019;291(3):781-91.
5. Busch F, Hoffmann L, Dos Santos DP, Makowski MR, Saba L, Prucker P, et al. Large language models for structured reporting in radiology: past, present, and future. *European Radiology*. 2024;1-14.
6. Doshi R, Amin KS, Khosla P, Bajaj SS, Chheang S, Forman HP. Quantitative evaluation of large language models to streamline radiology report impressions: A multimodal retrospective analysis. *Radiology*. 2024;310(3):e231593.
7. Reichenpfader D, Müller H, Denecke K. A scoping review of large language model-based approaches for information extraction from radiology reports. *NPJ Digital Medicine*. 2024;7(1):222.
8. Nowak S, Wulff B, Layer YC, Theis M, Isaak A, Salam B, et al. Privacy-ensuring open-weights large language models are competitive with closed-weights GPT-4o in extracting chest radiography findings from free-text reports. *Radiology*. 2025;314(1):e240895.

9. Shmidman S, Shmidman A, Cohen AD, Koppel M. Adapting LLMs to Hebrew: Unveiling DictaLM 2.0 with Enhanced Vocabulary and Instruction Capabilities. arXiv preprint arXiv:240707080. 2024.
10. Rivera M, Godbout JF, Rabbany R, Pelrine K. Combining Confidence Elicitation and Sample-based Methods for Uncertainty Quantification in Misinformation Mitigation. arXiv preprint arXiv:2401.08694. 2024.
11. Xiong M, Hu Z, Lu X, Li Y, Fu J, He J, et al. Can LLMs Express Their Uncertainty? An Empirical Evaluation of Confidence Elicitation in LLMs. arXiv preprint arXiv:2306.13063. 2024.
12. Zhou K, Jurafsky D, Hashimoto T. Navigating the Grey Area: How Expressions of Uncertainty and Overconfidence Affect Language Models. arXiv preprint arXiv:2302.13439. 2023.
13. Tonolini F, Massiah J, Aletras N, Kazai G. Bayesian prompt ensembles: Model uncertainty estimation for black-box large language models. Amazon Science. 2024.
14. Xi Z, Chen W, Guo X, He W, Ding Y, Hong B, et al. The rise and potential of large language model-based agents: A survey. arXiv preprint arXiv:230907864. 2023.
15. Friedman MY, Leventer-Roberts M, Rosenblum J, Zigman N, Goren I, Mourad V, et al. Development and validation of novel algorithms to identify patients with inflammatory bowel diseases in Israel: an epi-IIRN group study. *Clinical Epidemiology*. 2018;671-81.
16. Bruining DH, Zimmermann EM, Loftus Jr EV, Sandborn WJ, Sauer CG, Strong SA, et al. Consensus recommendations for evaluation, interpretation, and utilization of computed tomography and magnetic resonance enterography in patients with small bowel Crohn's disease. *Radiology*. 2018;286(3):776-99.

17. Hazan L, Focht G, Gavriellov N, Reichart R, Friss C, Cytter Kuint R, et al. P269 Harnessing Natural Language Processing for Structured Information Extraction from Radiology Reports in Crohn's Disease: A Nationwide Study From the epi-IIRN. *Journal of Crohn's and Colitis*. 2024;18(Supplement 1):i633-4.
18. Hazan L, Focht G, Gavriellov N, Reichart R, Hagopian T, Greer MLC, et al. Leveraging Prompt-Learning for Structured Information Extraction from Crohn's Disease Radiology Reports in a Low-Resource Language. arXiv preprint arXiv:240501682. 2024.
19. AI@Meta. Llama 3 Model Card; 2024. Available from: [https://github.com/meta-llama/llama-models/blob/main/models/llama3\\_1/MODEL\\_CARD.md](https://github.com/meta-llama/llama-models/blob/main/models/llama3_1/MODEL_CARD.md).
20. Vaswani A, Shazeer N, Parmar N, Uszkoreit J, Jones L, Gomez AN, et al. Attention Is All You Need. arXiv preprint arXiv:1706.03762. 2017.
21. Sun H. Supervised Fine-Tuning as Inverse Reinforcement Learning. arXiv preprint arXiv:2403.12017. 2024.
22. Christiano PF, Leike J, Brown T, Martic M, Legg S, Amodei D. Deep Reinforcement Learning from Human Preferences. *Advances in Neural Information Processing Systems*. 2017.
23. Stiennon N, Ouyang L, Wu J, Ziegler DM, Lowe R, Voss C, et al. Learning to summarize from human feedback. arXiv preprint arXiv:2009.01325. 2022.
24. Ouyang L, Wu J, Jiang X, Almeida D, Wainwright CL, Mishkin P, et al. Training language models to follow instructions with human feedback. arXiv preprint arXiv:2203.02155. 2022.
25. OpenAI. ChatGPT (GPT-4); 2024. Available from: <https://chat.openai.com>.

26. Zeng F, Lyu Z, Li Q, Li X. Enhancing LLMs for Impression Generation in Radiology Reports through a Multi-Agent System. arXiv preprint arXiv:241206828. 2024.

## **Figure captions:**

**Fig. 1:** (a) Distribution of organ-specific findings and (b) filtered organ-finding combinations

with more than 15 positive cases.

**Fig. 2:** Illustration of the proposed Bayesian Prompt Ensemble pipeline for uncertainty-aware predictions. A radiology report and multiple semantically equivalent prompts are fed into an LLM, generating one prediction per prompt. These predictions are then aggregated to yield a final decision and uncertainty estimation. The aggregation function can be either an LLM agent or an entropy-based function that applies uniform weights, learned fixed weights, or weights predicted by a pre-trained MLP model.

**Fig. 3:** Uncertainty Histograms for Ileum stenosis Computed by: (a) Uniform Weights, (b) Linear-Optimized Weights, (c) Learnable- MLP Weights, and (d) Agent-based decision.

**Fig. 4:** Uncertainty Histograms for Ileum inflammation Computed by: (a) Uniform Weights, (b) Linear-Optimized Weights, (c) Learnable- MLP Weights, and (d) Agent-based decision.

**Table 1:** Comparison of average results across all labels for different methods before applying the uncertainty threshold.

Model	Accuracy	F1	Precision	Recall	Kappa
<b>Baseline</b>	0.8243	0.2699	0.3046	0.3097	0.179
<b>Uniform</b>	0.832	0.3873	0.336	0.5336	0.2979
<b>Linear</b>	0.8454	0.3847	0.3463	0.4878	0.2988
<b>MLP</b>	<b>0.8605</b>	0.3643	<b>0.3772</b>	0.3977	0.2863
<b>Agent</b>	0.8022	<b>0.3967</b>	0.3131	<b>0.6437</b>	<b>0.3006</b>

**Table 2:** Comparison of average of the median uncertainty values, across all 23 labels, for correct and incorrect predictions across different methods.

Method	Median Uncertainty	
	Correct Predictions	Incorrect Predictions
Uniform	0.4081	0.6153
Linear	0.2668	0.4694
MLP	0.2261	0.5717
Agent	<b>0</b>	<b>0.5108</b>

**Table 3:** Comparison of average results across all labels for different methods after applying uncertainty threshold  $\geq 0.5$ .

Model	Accuracy	F1	Precision	Recall	Kappa	Excluded Cases
Baseline	0.8243	0.2699	0.3046	0.3097	0.179	0
Uniform	0.9188	0.4634	0.4458	0.5327	0.4203	200 (43.31%)
Linear	0.897	0.4261	0.4008	0.508	0.3702	96 (20.97%)
MLP	<b>0.9242</b>	0.4032	<b>0.4584</b>	0.4079	0.3643	120 (26.07%)
Agent	0.8947	<b>0.4787</b>	0.3976	<b>0.6614</b>	<b>0.4258</b>	153 (33.16%)

**Table 4:** Comparison of average results across all labels for different methods after applying uncertainty threshold up to  $\geq 0.5$ , with case exclusions limited to a maximum of 20%.

Model	Accuracy	F1	Precision	Recall	Kappa	Excluded Cases
Baseline	0.8243	0.2699	0.3046	0.3097	0.179	0
Uniform	0.8789	0.4267	0.3873	0.5304	0.3615	92 (19.91%)
Linear	0.8905	0.212	0.3938	0.5079	0.3613	80 (17.5%)
MLP	<b>0.9087</b>	0.3933	<b>0.4492</b>	0.4004	0.345	90 (19.5%)
Agent	0.8285	<b>0.4494</b>	0.3529	<b>0.7295</b>	<b>0.3683</b>	92 (19.91%)

## **Appendix A**

**Table S1:** HSMP-BERT performances for the 23 selected labels on the test-set. The selected labels for the MLP training (Kappa>0.7) are highlighted.

Label	Accuracy	Precision	Recall	F1	Kappa	Roc-AUC
Cecum inflammation	0.9310	0.7730	0.6573	0.6959	0.3950	0.6573
Cecum wall enhancement	0.9483	0.6865	0.6865	0.6865	0.3730	0.6865
Cecum wall thickness	0.9569	0.8240	0.8611	0.8413	0.6827	0.8611
Colon inflammation	0.9052	0.8228	0.7739	0.7952	0.5910	0.7739
Colon mesenteric edema or fat stranding	0.9569	0.4784	0.5000	0.4890	0.0000	0.5000
Colon wall enhancement	0.9310	0.8061	0.6906	0.7432	0.6056	0.6906
Colon wall thickness	0.9310	0.8394	0.8134	0.8469	0.6945	0.8134
<b>Ileum comb sign</b>	0.9483	0.9135	0.8723	0.8913	0.7826	0.8723
Ileum fistula	0.9397	0.7808	0.9146	0.8318	0.6639	0.9146
<b>Ileum inflammation</b>	0.8793	0.8745	0.8787	0.8763	0.7527	0.8787
Ileum mesenteric edema or fat stranding	0.8966	0.8667	0.6513	0.6970	0.6113	0.6513
<b>Ileum pre-stenotic dilation</b>	0.9569	0.9212	0.9366	0.9286	0.8573	0.9366
Ileum reduced motility	0.9828	0.9912	0.7500	0.8290	0.6588	0.7500
<b>Ileum stenosis</b>	0.9224	0.8884	0.9138	0.9008	0.8000	0.9138
<b>Ileum wall enhancement</b>	0.9569	0.9514	0.9559	0.9536	0.9072	0.9559
<b>Ileum wall thickness</b>	0.9397	0.9417	0.9444	0.9396	0.8797	0.9444
Rectum inflammation	0.9397	0.8482	0.6620	0.7148	0.4345	0.6620
Rectum wall enhancement	0.9714	0.9867	0.7500	0.8261	0.6548	0.7500
<b>Rectum wall thickness</b>	0.9828	0.9910	0.8571	0.9121	0.8245	0.8571
<b>Sigmoid comb sign</b>	0.9914	0.9956	0.8333	0.8978	0.7958	0.8333
Sigmoid inflammation	0.8793	0.7484	0.6938	0.7157	0.4330	0.6938
Sigmoid wall enhancement	0.9310	0.7730	0.6573	0.6959	0.3950	0.6573
Sigmoid wall thickness	0.9483	0.9144	0.7869	0.8358	0.6729	0.7869

## Appendix B

### The different prompts used to query the LLM for the data in the radiology report.

Does the following radiology report indicate that the patient has *{label}*? Here is the report: *{report}*. Answer shortly, format your answer as a JSON file using the following schema: {"Answer": "Yes/No", "Explanation": "str"}. Important: Only return a single piece of valid JSON text. For example: {"Answer": "Yes", "Explanation": "The report mentions that the patient has a severe case of the disease."}

Does the radiology report below suggest that the patient is suffering from *{label}*? Here is the report: *{report}*. Please provide a concise answer, formatted as a JSON object using the following schema: {"Answer": "Yes/No", "Explanation": "str"}. Important: Ensure you return a single valid JSON object. For instance: {"Answer": "Yes", "Explanation": "The report indicates that the patient has severe symptoms of the condition."}

Can the presence of *{label}* be confirmed from the following radiology report? Here is the report: *{report}*. Provide a brief response, formatted as a JSON object according to the following schema: {"Answer": "Yes/No", "Explanation": "str"}. Important: Only return a single valid JSON object.

Does the patient appear to have *{label}* based on the analysis of the radiology report provided? Here is the report: *{report}*. Please answer succinctly, formatted as a JSON object in the following schema: {"Answer": "Yes/No", "Explanation": "str"}. Important: Return only a single valid JSON object. For example: {"Answer": "Yes", "Explanation": "The report clearly states that the patient has a significant case of the condition."}

Considering the radiology report presented, is there an indication that the patient has *{label}*? Here is the report: *{report}*. Provide a brief answer, formatted as a JSON object according to the schema: {"Answer": "Yes/No", "Explanation": "str"}. Important: Make sure to return a single valid JSON object. For instance: {"Answer": "Yes", "Explanation": "The report notes that the patient shows clear signs of the condition."}

Is it possible to conclude from the following radiology report that the patient has *{label}*? Here is the report: *{report}*. Please provide a concise response, formatted as a JSON object using the schema: {"Answer": "Yes/No", "Explanation": "str"}. Important: Ensure only a single valid JSON object is returned. For instance: {"Answer": "Yes", "Explanation": "The report suggests that the patient has a pronounced case of the condition."}

## Appendix C

Comparison Results for Different Uncertainty Thresholding.

**Table S2:** Comparison of different methods before filtering using uncertainty threshold.

Label	prevalence	F1 Score [%]					Accuracy [%]					Kappa [%]				
		Baseline	Uniform	Linear	MLP	Agent	Baseline	Uniform	Linear	MLP	Agent	Baseline	Uniform	Linear	MLP	Agent
Cecum inflammation	8.22%	25.415	28.148	29.508	28.829	33.083	83.117	79.004	81.385	82.900	80.736	0.169	0.185	0.205	0.202	0.242
Cecum wall enhancement	4.54%	9.525	12.000	12.048	11.429	11.475	84.776	80.952	84.199	86.580	76.623	0.034	0.052	0.056	0.054	0.043
Cecum wall thickness	6.49%	24.929	32.759	31.858	32.911	27.419	85.426	83.117	83.333	88.528	80.519	0.181	0.256	0.247	0.270	0.195
Colon inflammation	15.15%	37.020	44.954	44.118	42.786	43.478	77.633	74.026	75.325	75.108	69.048	0.239	0.307	0.302	0.287	0.276
Colon mesenteric edema or fat stranding	3.24%	4.893	8.889	10.000	13.793	18.667	91.522	91.126	92.208	94.589	86.797	0.016	0.048	0.062	0.110	0.142
Colon wall enhancement	8.22%	16.365	23.913	24.390	20.290	28.788	84.632	84.848	86.580	88.095	79.654	0.091	0.158	0.171	0.139	0.193
Colon wall thickness	12.77%	29.524	41.905	39.604	38.636	45.802	84.127	86.797	86.797	88.312	84.632	0.214	0.346	0.324	0.330	0.370
Ileum comb sign	14.50%	28.299	41.808	39.216	31.746	42.927	77.814	77.706	79.870	81.385	74.675	0.165	0.290	0.274	0.210	0.291
Ileum fistula	6.27%	33.782	48.421	51.282	54.286	43.137	87.879	89.394	91.775	93.074	87.446	0.282	0.435	0.471	0.507	0.375
Ileum inflammation	41.77%	60.544	86.162	84.182	84.615	86.978	73.846	88.528	87.229	87.879	88.528	0.430	0.764	0.735	0.747	0.768
Ileum mesenteric edema or fat stranding	11.90%	17.608	34.000	26.966	26.506	36.842	84.488	85.714	85.931	86.797	84.416	0.105	0.261	0.197	0.201	0.280
Ileum pre-stenotic dilation	16.01%	27.070	40.816	42.105	40.698	39.583	73.052	68.615	71.429	77.922	62.338	0.121	0.238	0.261	0.275	0.207
Ileum reduced motility	2.81%	17.169	26.316	33.333	28.000	20.000	87.518	87.879	92.208	92.208	82.684	0.135	0.227	0.304	0.249	0.159
Ileum stenosis	22.07%	39.536	56.585	53.608	53.631	64.655	78.571	80.736	80.519	82.035	82.251	0.278	0.442	0.413	0.428	0.530
Ileum wall enhancement	31.88%	40.055	65.815	70.414	50.000	67.630	68.872	76.790	78.308	73.102	75.705	0.212	0.483	0.537	0.325	0.489
Ileum wall thickness	42.85%	56.885	79.656	77.551	73.457	88.384	72.367	84.632	83.333	81.385	90.043	0.399	0.677	0.648	0.602	0.797
Rectum inflammation	7.14%	21.380	27.273	28.261	31.461	26.087	85.281	82.684	85.714	86.797	77.922	0.140	0.192	0.210	0.247	0.171
Rectum wall enhancement	3.67%	8.962	20.690	18.868	11.765	20.690	89.935	90.043	90.693	93.506	85.065	0.051	0.163	0.146	0.084	0.157
Rectum wall thickness	5.84%	25.029	33.803	29.730	37.736	36.893	89.610	89.827	88.745	92.857	85.931	0.200	0.286	0.241	0.339	0.309
Sigmoid comb sign	3.46%	16.065	21.918	25.000	18.868	18.367	88.348	87.662	90.909	90.693	82.684	0.117	0.175	0.211	0.147	0.133
Sigmoid inflammation	12.55%	29.698	40.000	37.255	39.362	36.015	75.433	71.429	72.294	75.325	63.853	0.164	0.264	0.235	0.266	0.205
Sigmoid wall enhancement	7.14%	17.963	27.368	23.377	23.729	33.824	84.957	85.065	87.229	90.260	80.519	0.112	0.199	0.166	0.186	0.258
Sigmoid wall thickness	11.03%	33.069	47.788	52.252	43.373	41.791	86.869	87.229	88.528	89.827	83.117	0.264	0.406	0.458	0.381	0.326

**Table S3:** Comparison of different methods after filtering using uncertainty threshold < 0.5.

Label	F1 Score					Accuracy					Kappa					Cases				
	Baseline	Uniform	Linear	MLP	Agent	Baseline	Uniform	Linear	MLP	Agent	Baseline	Uniform	Linear	MLP	Agent	Baseline	Uniform	Linear	MLP	Agent
Cecum inflammation	25.415	37.209	28.571	35.294	33.333	83.117	90.217	88.439	93.060	88.991	0.169	0.324	0.235	0.317	0.291	462	276	346	317	327
Cecum wall enhancement	9.525	14.286	15.385	7.143	13.636	84.776	90.123	87.978	92.145	88.013	0.034	0.104	0.101	0.030	0.089	462	243	366	331	317
Cecum wall thickness	24.929	59.259	47.619	41.667	40	85.426	95.971	93.189	95.796	91.429	0.181	0.573	0.442	0.395	0.363	462	273	323	333	315
Colon inflammation	37.020	54.237	49.645	51.724	51.701	77.633	81.315	80.759	83.673	77.389	0.239	0.437	0.391	0.423	0.399	462	289	369	343	314
Colon mesenteric edema or fat stranding	4.893	20	18.182	26.667	28.571	91.522	97.403	95.522	97.158	95.268	0.016	0.187	0.159	0.255	0.264	462	308	402	387	317
Colon wall enhancement	16.365	14.815	22.222	16.216	17.021	84.632	91.513	89.231	91.507	87.171	0.091	0.104	0.165	0.122	0.110	462	271	390	365	304
Colon wall thickness	29.524	53.333	46.667	39.024	58.182	84.127	94.928	91.557	93.075	92.557	0.214	0.507	0.423	0.366	0.541	462	276	379	361	309
Ileum comb sign	28.299	50	33.803	44.898	45.070	77.814	91.111	86.610	91.589	84.337	0.165	0.451	0.264	0.404	0.369	462	180	351	321	249
Ileum fistula	33.782	72.727	52.381	68.966	71.795	87.879	96.774	95.025	97.656	96.440	0.282	0.710	0.500	0.678	0.700	462	279	402	384	309
Ileum inflammation	60.544	93.103	87.719	89.270	96.350	73.846	94.595	90.814	92.795	97.093	0.430	0.887	0.804	0.839	0.939	462	296	381	347	344
Ileum mesenteric edema or fat stranding	17.608	16.667	27.451	0	33.333	84.488	93.174	90.339	92.800	92.429	0.105	0.140	0.229	-0.010	0.294	462	293	383	375	317
Ileum pre-stenotic dilation	27.070	60.606	55.285	55.072	47.788	73.052	84.049	81.544	87.398	75.918	0.121	0.512	0.448	0.480	0.355	462	163	298	246	245
Ileum reduced motility	17.169	40	32	33.333	44.444	87.518	96.203	95.550	97.640	94.604	0.135	0.385	0.303	0.323	0.421	462	237	382	339	278
Ileum stenosis	39.536	69.231	62.069	57.971	79.245	78.571	91.367	87.912	91.265	92.994	0.278	0.642	0.549	0.535	0.751	462	278	364	332	314
Ileum wall enhancement	40.055	69.565	73.548	57.143	67.114	68.872	85.641	83.730	86.121	82.182	0.212	0.603	0.620	0.489	0.556	461	195	252	281	275
Ileum wall thickness	56.885	91.971	83.810	81.633	95.575	72.367	95.492	90.368	91.641	96.960	0.399	0.888	0.771	0.764	0.933	462	244	353	323	329
Rectum inflammation	21.380	36.842	32.877	38.095	36.923	85.281	91.549	88.305	92.614	87.538	0.140	0.325	0.269	0.342	0.310	462	284	419	352	329
Rectum wall enhancement	8.962	0	20.690	0	28.571	89.935	94.872	94.148	96.296	93.528	0.051	-0.026	0.178	-0.017	0.261	462	273	393	378	309
Rectum wall thickness	25.029	58.824	40	38.095	50	89.610	97.569	94.167	96.359	93.902	0.200	0.576	0.370	0.364	0.471	462	288	360	357	328
Sigmoid comb sign	16.065	18.750	20.513	23.077	32.432	88.348	90.780	92.512	94.565	92.447	0.117	0.146	0.174	0.204	0.291	462	282	414	368	331
Sigmoid inflammation	29.698	42.222	43.548	43.478	45.763	75.433	78.151	79.290	82.253	77.224	0.164	0.319	0.335	0.346	0.350	462	238	338	293	281
Sigmoid wall enhancement	17.963	31.579	35.294	31.250	32	84.957	94.961	93.732	93.872	89.032	0.112	0.290	0.320	0.281	0.269	462	258	351	359	310
Sigmoid wall thickness	33.069	60.606	50.847	47.368	52.174	86.869	95.652	92.388	94.490	90.571	0.264	0.584	0.468	0.450	0.470	462	299	381	363	350

**Table S4:** Comparison of different methods after filtering up to 20% of the data, using uncertainty threshold < 0.5.

Label	F1 Score					Accuracy					Kappa					Cases				
	Baseline	Uniform	Linear	MLP	Agent	Baseline	Uniform	Linear	MLP	Agent	Baseline	Uniform	Linear	MLP	Agent	Baseline	Uniform	Linear	MLP	Agent
Cecum inflammation	25.415	31.325	33.333	35.088	36.364	83.117	84.595	88.108	90	82.973	0.169	0.245	0.277	0.299	0.294	462	370	370	370	370
Cecum wall enhancement	9.525	15.625	15.385	15	14.894	84.776	85.405	88.108	90.811	78.378	0.034	0.095	0.102	0.103	0.083	462	370	370	370	370
Cecum wall thickness	24.929	38.710	42.623	35.897	30.928	85.426	89.730	90.541	93.243	81.892	0.181	0.342	0.379	0.324	0.244	462	370	370	370	370
Colon inflammation	37.020	49.080	49.296	50	50.256	77.633	77.568	80.541	81.622	73.784	0.239	0.363	0.387	0.394	0.362	462	370	370	370	370
Colon mesenteric edema or fat stranding	4.893	16.667	18.182	26.667	17.857	91.522	94.595	95.522	97.158	87.568	0.016	0.140	0.159	0.255	0.137	462	370	402	387	370
Colon wall enhancement	16.365	28.070	22.222	16.216	30.189	84.632	88.919	89.231	91.622	80	0.091	0.221	0.165	0.122	0.212	462	370	390	370	370
Colon wall thickness	29.524	47.761	46.667	40.909	54.902	84.127	90.541	91.557	92.973	87.568	0.214	0.427	0.423	0.383	0.481	462	370	379	370	370
Ileum comb sign	28.299	41.584	35.443	36.620	47.853	77.814	84.054	86.216	87.838	77.027	0.165	0.329	0.277	0.300	0.358	462	370	370	370	370
Ileum fistula	33.782	65.385	52.381	68.966	53.012	87.879	95.135	95.025	97.656	89.459	0.282	0.629	0.500	0.678	0.481	462	370	402	384	370
Ileum inflammation	60.544	90.604	87.719	88.281	92.652	73.846	92.432	90.814	91.892	93.784	0.430	0.843	0.804	0.821	0.873	462	370	381	370	370
Ileum mesenteric edema or fat stranding	17.608	29.787	27.451	0	45.977	84.488	91.081	90.339	92.800	87.297	0.105	0.252	0.229	-0.010	0.389	462	370	383	375	370
Ileum pre-stenotic dilation	27.070	46.154	46.707	46.667	43.902	73.052	73.514	75.946	82.703	62.703	0.121	0.314	0.339	0.367	0.243	462	370	370	370	370
Ileum reduced motility	17.169	31.579	32	37.500	21.687	87.518	92.973	95.550	97.297	82.432	0.135	0.289	0.303	0.363	0.174	462	370	382	370	370
Ileum stenosis	39.536	63.704	61.667	60.606	76.471	78.571	86.757	87.568	89.459	89.189	0.278	0.556	0.543	0.549	0.696	462	370	370	370	370
Ileum wall enhancement	40.055	66.964	72.797	53.988	74.126	68.872	79.946	80.759	79.675	79.946	0.212	0.527	0.583	0.412	0.585	461	369	369	369	369
Ileum wall thickness	56.885	86.853	83.700	79.245	93.836	72.367	91.081	90	88.108	95.135	0.399	0.802	0.766	0.713	0.898	462	370	370	370	370
Rectum inflammation	21.380	38.095	32.877	36	29.167	85.281	89.459	88.305	91.351	81.622	0.140	0.327	0.269	0.314	0.211	462	370	419	370	370
Rectum wall enhancement	8.962	7.692	20.690	0	23.188	89.935	93.514	94.148	96.296	85.676	0.051	0.045	0.178	-0.017	0.191	462	370	393	378	370
Rectum wall thickness	25.029	42.857	41.026	36.364	44.706	89.610	93.514	93.784	96.216	87.297	0.200	0.394	0.378	0.347	0.390	462	370	370	370	370
Sigmoid comb sign	16.065	18.182	20.513	23.077	23.529	88.348	90.270	92.512	94.595	85.946	0.117	0.144	0.174	0.204	0.189	462	370	414	370	370
Sigmoid inflammation	29.698	39.752	43.662	40.310	41.475	75.433	73.784	78.378	79.189	65.676	0.164	0.272	0.331	0.300	0.256	462	370	370	370	370
Sigmoid wall enhancement	17.963	33.333	31.579	28.571	37.383	84.957	90.270	92.973	93.243	81.892	0.112	0.284	0.279	0.251	0.293	462	370	370	370	370
Sigmoid wall thickness	33.069	51.724	50.847	48.780	49.412	86.869	92.432	92.388	94.324	88.378	0.264	0.477	0.468	0.463	0.430	462	370	381	370	370

## Appendix D

Uncertainty histograms.

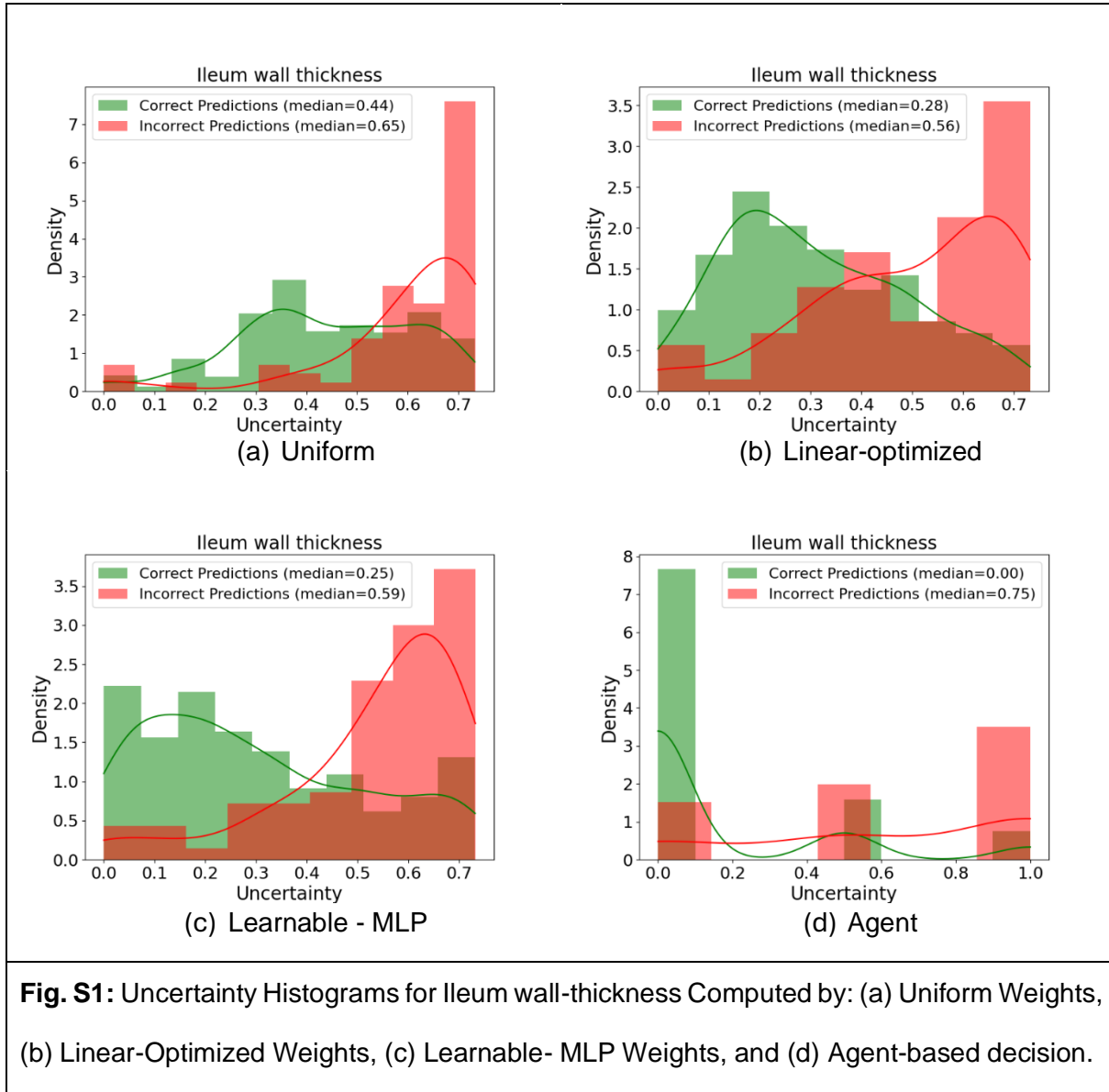


**Fig. S1:** Uncertainty Histograms for Ileum wall-thickness Computed by: (a) Uniform Weights, (b) Linear-Optimized Weights, (c) Learnable- MLP Weights, and (d) Agent-based decision.

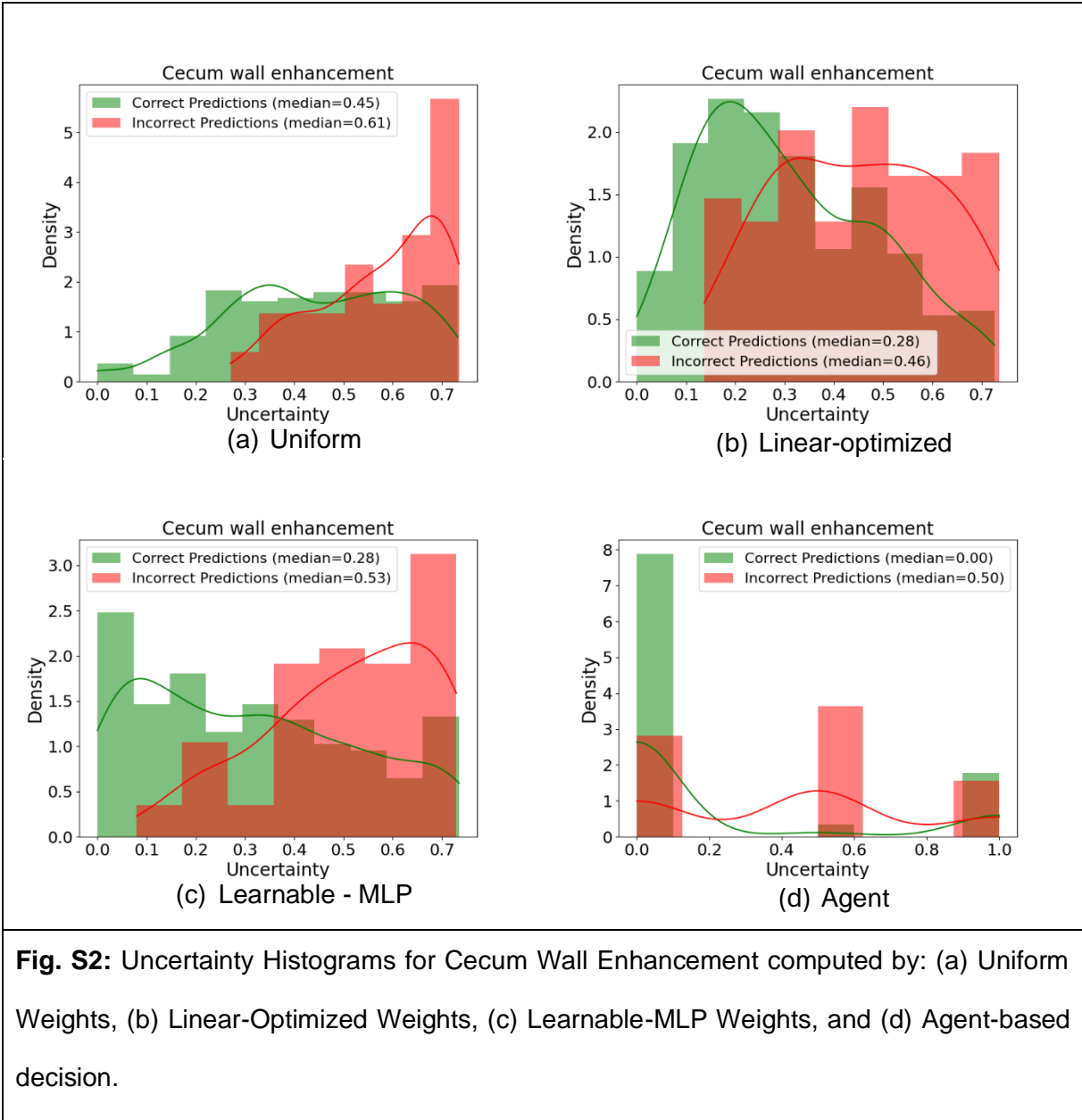


**Fig. S2:** Uncertainty Histograms for Cecum Wall Enhancement computed by: (a) Uniform Weights, (b) Linear-Optimized Weights, (c) Learnable-MLP Weights, and (d) Agent-based decision.

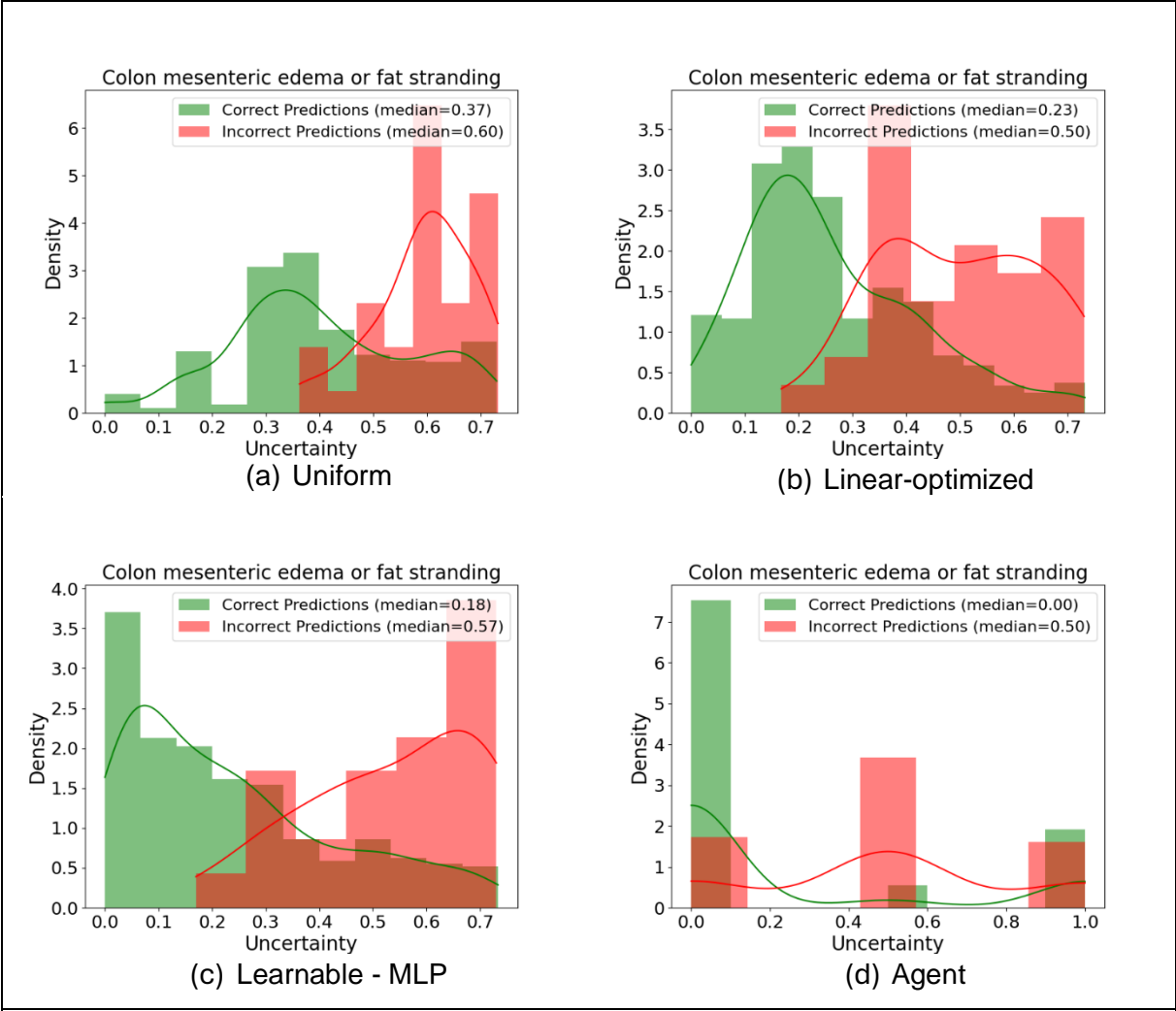


**Fig. S3:** Uncertainty Histograms for Colon Mesenteric Edema or Fat Stranding computed by: (a) Uniform Weights, (b) Linear-Optimized Weights, (c) Learnable-MLP Weights, and (d) Agent-based decision.

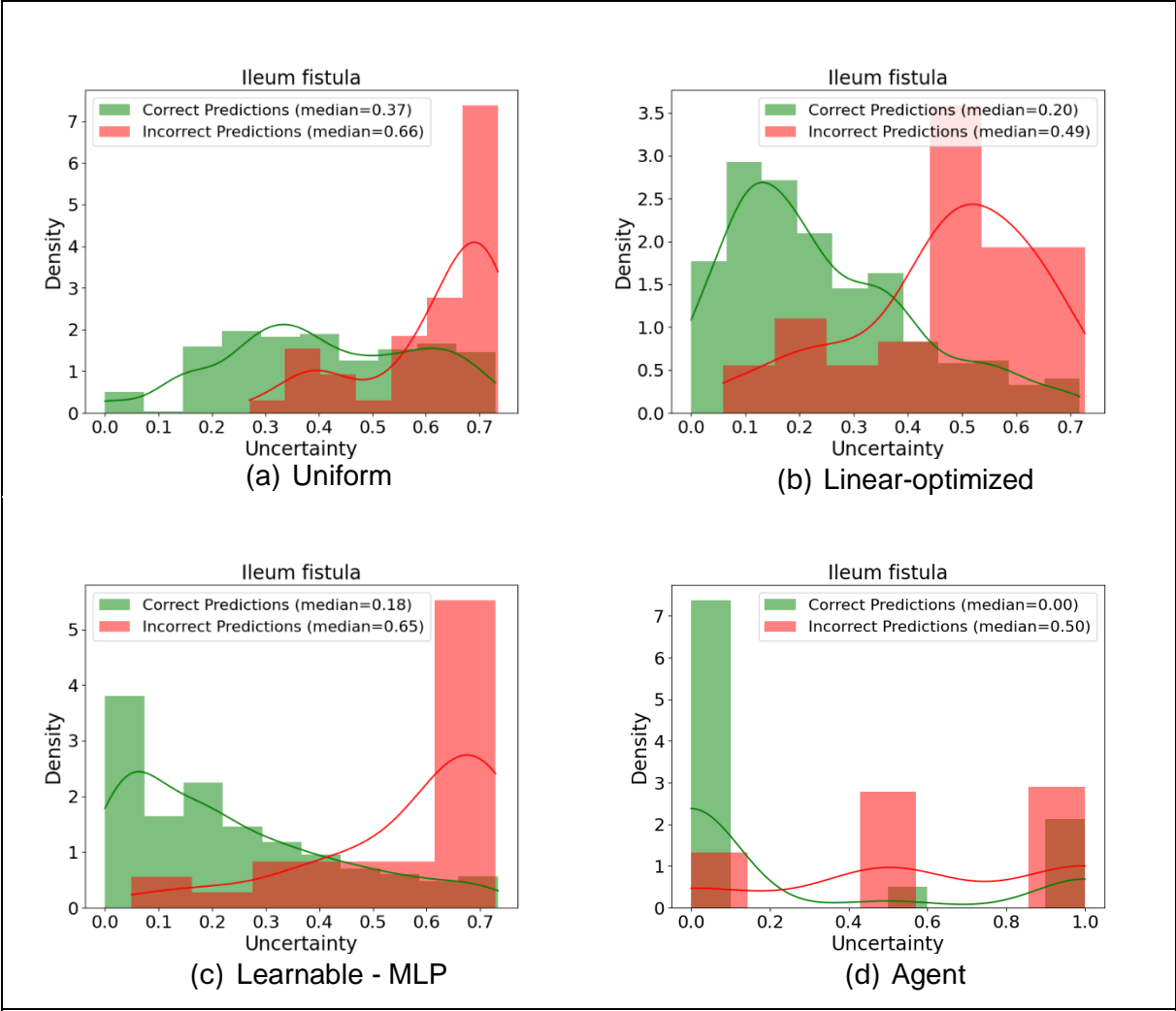


**Fig. S4:** Uncertainty Histograms for Ileum fistula computed by: (a) Uniform Weights, (b) Linear-Optimized Weights, (c) Learnable-MLP Weights, and (d) Agent-based decision.

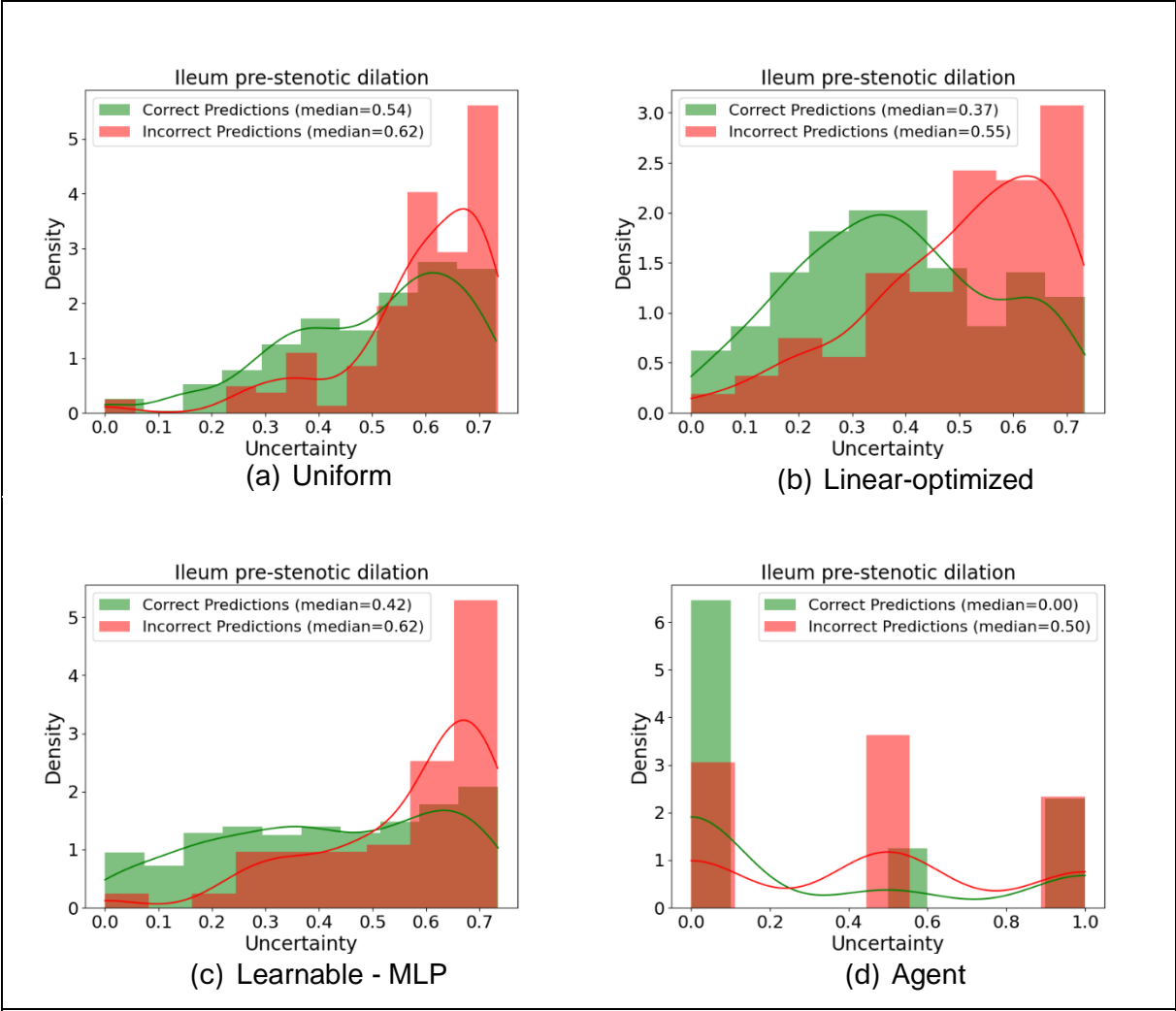


**Fig. S5:** Uncertainty Histograms for Ileum pre-stenotic dilation computed by: (a) Uniform Weights, (b) Linear-Optimized Weights, (c) Learnable-MLP Weights, and (d) Agent-based decision.

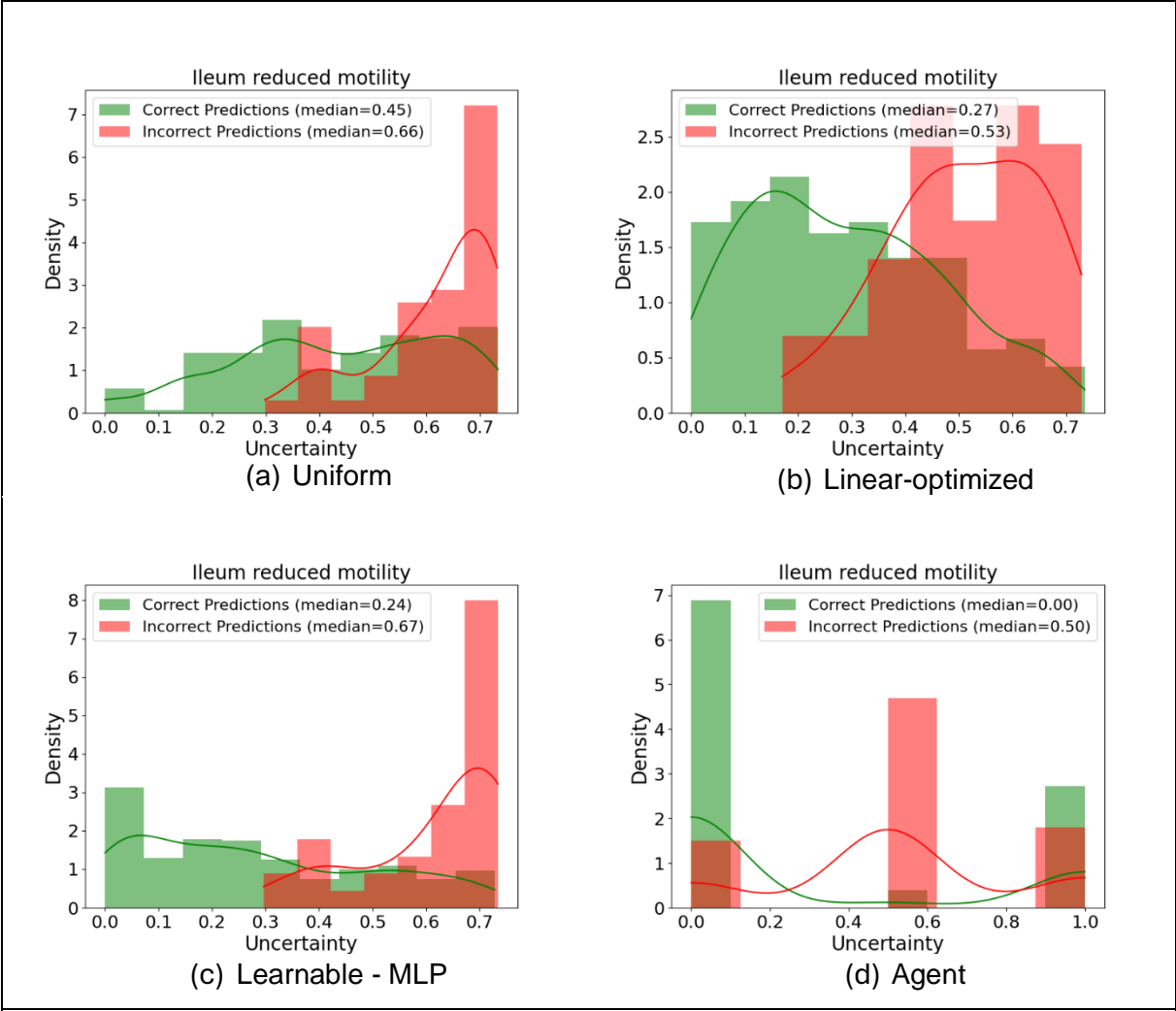


**Fig. S6:** Uncertainty Histograms for Ileum reduced motility computed by: (a) Uniform Weights, (b) Linear-Optimized Weights, (c) Learnable-MLP Weights, and (d) Agent-based decision.

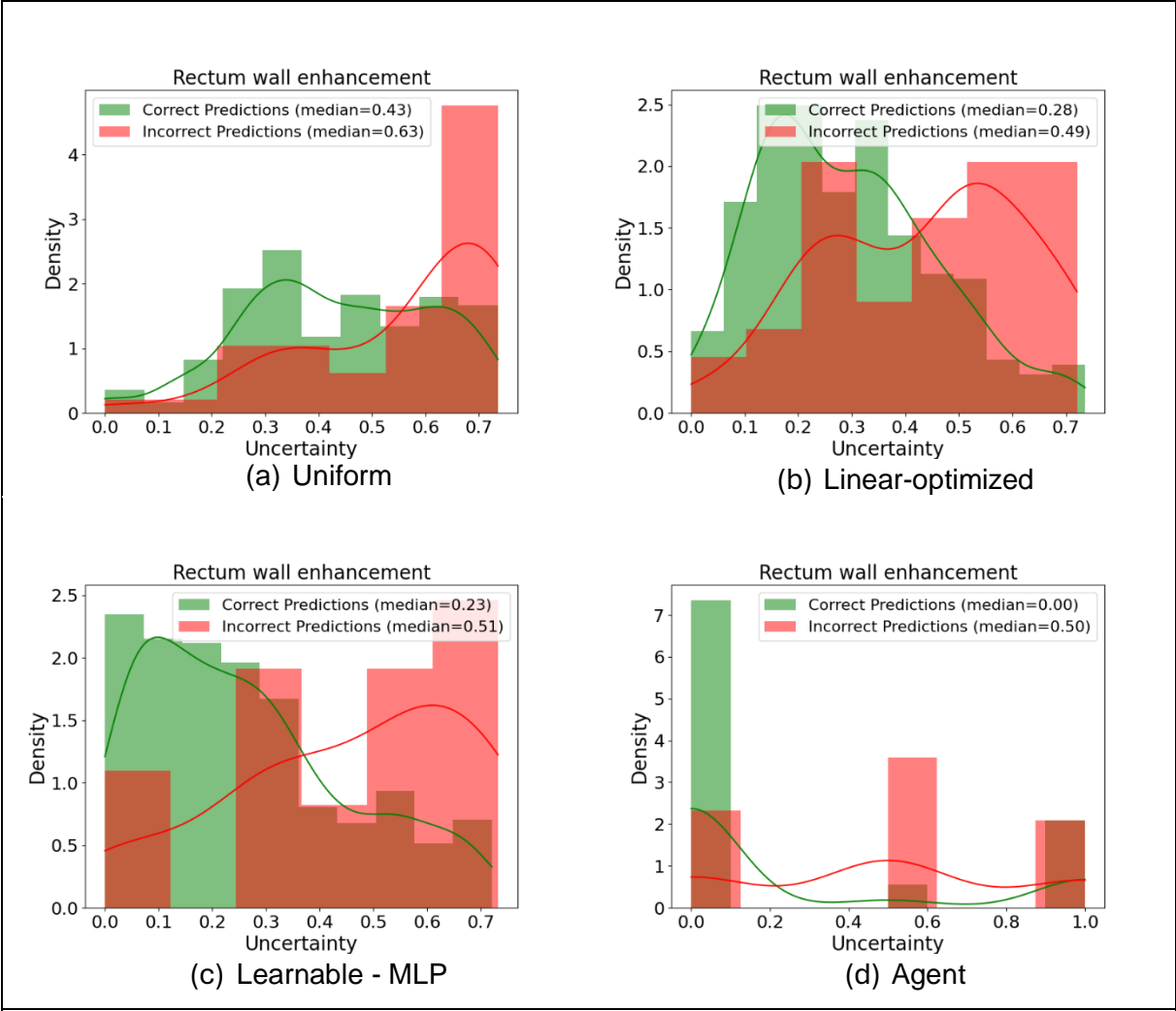


**Fig. S7:** Uncertainty Histograms for Rectum Wall Enhancement computed by: (a) Uniform Weights, (b) Linear-Optimized Weights, (c) Learnable-MLP Weights, and (d) Agent-based decision.

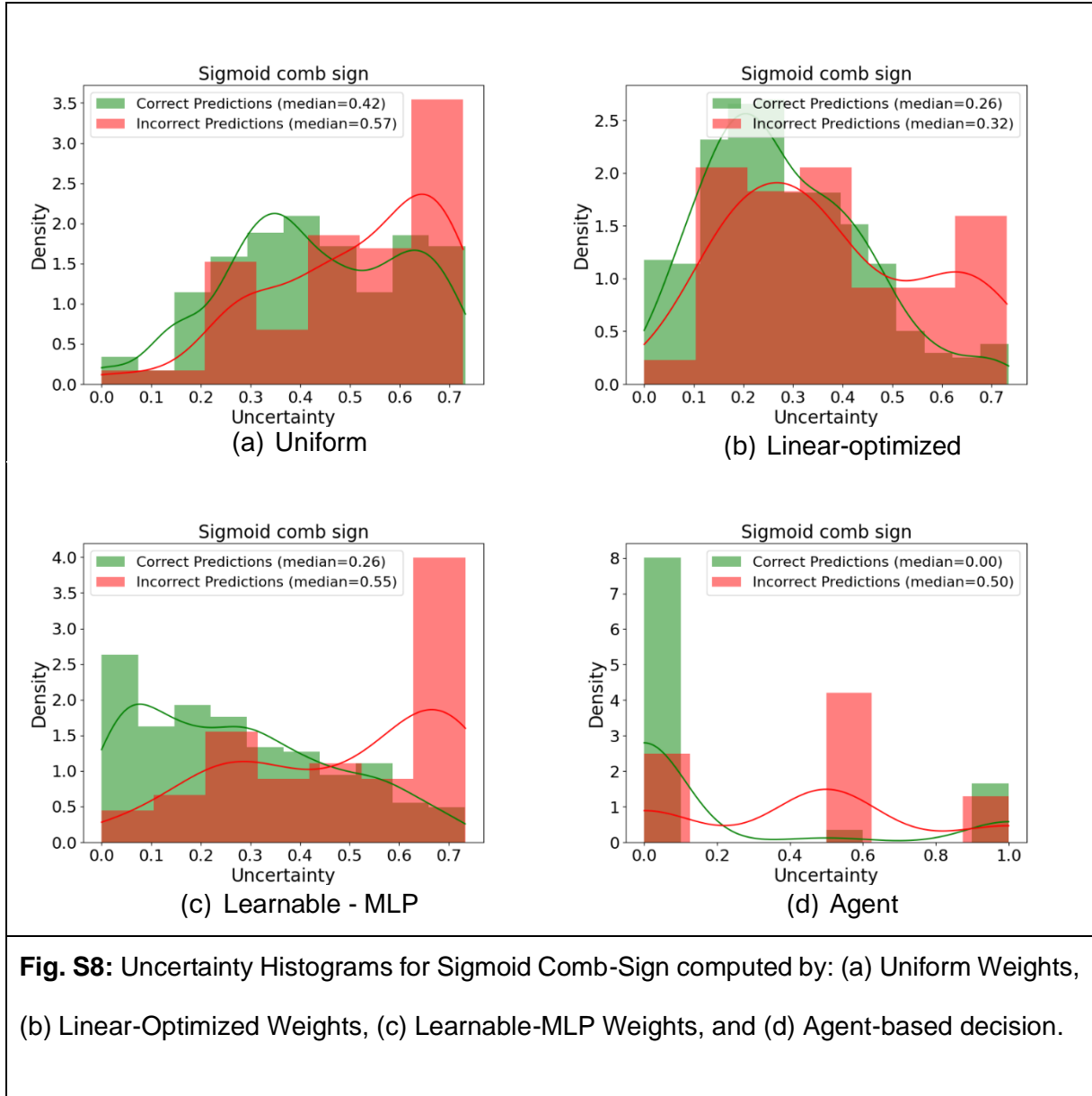


**Fig. S8:** Uncertainty Histograms for Sigmoid Comb-Sign computed by: (a) Uniform Weights, (b) Linear-Optimized Weights, (c) Learnable-MLP Weights, and (d) Agent-based decision.